RSC Advances

PAPER

View Article Online
View Journal | View Issue

Cite this: *RSC Adv.*, 2021, **11**, 8117

MOF-derived zirconia-supported Keggin heteropoly acid nanoporous hybrids as a reusable catalyst for methyl oleate production†

Qiuyun Zhang, *[ab] Dandan Lei,[a] Qizhi Luo,[a] Xianju Yang,[a] Yaping Wu,[a] Jialu Wang[c] and Yutao Zhang*[ab]

Received 21st January 2021
Accepted 4th February 2021

DOI: 10.1039/d1ra00546d

rsc.li/rsc-advances

In this study, a series of nanoporous HSiW@ZrO_2 hybrids were synthesized using a zirconium metal–organic framework UiO-66 as a precursor towards biodiesel production. The structural and morphological properties of the obtained hybrids were characterized by the wide-angle XRD, FTIR, SEM, TEM, N_2 adsorption/desorption, and NH_3-TPD methods. Moreover, their catalytic activity in terms of calcination temperature during preparation was investigated, and the HSiW@ZrO_2 hybrids calcinated at 300 °C exhibited the highest activity and the oleic acid (OA) conversion of 94.0% owing to the presence of the relatively high surface area, appropriate pore size and strong acidity. It was also revealed that the hybrids maintained as high as 82.0% even after nine cycles. Intriguingly, the nanoporous catalysts were found to exhibit excellent catalytic activity towards the esterification of the high acid value of *Jatropha curcas* oil.

1. Introduction

Many decades ago, owing to global warming, environmental pollution was becoming severe and fossil fuel resources were increasingly exhausted,[1–3] while biodiesel, an eco-friendly and sustainable alternative fuel, with numerous favorable features such as non-toxic, low viscosity, biodegradable, high flash point, better lubrication, low emissions of greenhouse gases, and direct use in diesel engines without modification, has attracted sustained attention.[4] Biodiesel is usually produced through either transesterification or esterification depending on the various feedstocks. Among them, transesterification is a reaction between various oils (*e.g.*, soybean oil,[5] castor seed oil,[6] *Euphorbia lathyris* oil,[7] waste cooking oil[8]) and short-chain alcohols (*e.g.*, methanol and ethanol) in the presence of a catalyst to produce fatty acid alkyl esters and glycerol as a side product. Esterification converts different long-chain carboxylic acids (*e.g.*, oleic acid,[9] stearic acid,[10] and myristic acid[11]) and short-chain alcohols into esters and water as a co-product *via* an acid catalyst.

Nowadays, numerous catalytic systems such as homogeneous, heterogeneous and some enzymes are used in the esterification/transesterification reaction for the production of biodiesel. Among these, the homogeneous catalytic systems exhibited a fast reaction rate; however, some disadvantages in these systems are still significant, such as corrosive nature and nonregenerable.[12] Besides, the enzymatic catalytic systems are also commonly used in biodiesel production, but their practical applications are always limited by the poor stability and high cost.[13] Hence, the investigation of heterogeneous catalytic systems for the production of biodiesel recently has become a research hotspot owing to their high catalytic activity, stability, reusability and easy regeneration,[14] but heterogeneous base catalysts are not suitable for catalyzing free fatty acids and oils with high acid values due to saponification reactions.[15] To this end, several types of heterogeneous acid catalysts such as porous mixed oxides,[16] ionic liquids,[17] and carbon-based catalysts[18] have been proposed for the ease of regeneration and reuse. Unfortunately, the acid density and stability of these heterogeneous catalysts are always unsatisfactory.[15] Contrarily, heteropoly acids have advantages such as strong Brønsted acidity and special Keggin-type structural properties for acid-catalyzed reactions.[19,20] However, unsupported heteropoly acids have high solubility in polar media and low surface area, which limit their industrial applications.[21–23] Therefore, the design of heteropoly acids encapsulation into the excellent and stable porous supported for biodiesel production is still a great challenge.

Recently, some metal–organic frameworks (MOFs) with high specific surface area, controlled pore size, and structural diversity are used as precursors to prepare porous materials and applied as catalyst supports in many catalytic applications.[24,25] In the present study, UiO-66, a class of Zr-MOFs, was selected as Zr-based MOFs for the preparation of nanoporous HSiW@ZrO_2 hybrids, and the textural structure of the obtained hybrids has

[a]School of Chemistry and Chemical Engineering, Anshun University, Anshun, 561000, Guizhou, China. E-mail: qyzhang.asu@gmail.com

[b]Engineering Technology Center of Control and Remediation of Soil Contamination of Guizhou Science and Technology Department, Anshun University, Anshun, 561000, Guizhou, China. E-mail: zyt0516@126.com

[c]School of Resource and Environmental Engineering, Anshun University, Anshun, 561000, Guizhou, China

† Electronic supplementary information (ESI) available. See DOI: 10.1039/d1ra00546d

been extensively investigated by comparing with different calcination temperatures. Moreover, the catalytic performance of these HSiW@ZrO_2 hybrids for methyl oleate production *via* the esterification of oleic acid (OA) with methanol was also studied as well as investigated in the esterification of the high acid value of *Jatropha curcas* oil.

2. Experimental

2.1. Materials and synthesis

All chemicals were obtained from commercial sources and used without further purification. Zirconium(IV) chloride ($ZrCl_4$, AR), terephthalic acid (H_2-BDC) (AR), and silicotungstic acid (HSiW, $H_4SiW_{12}O_{40}\cdot nH_2O$, HSiW, AR) were purchased from Shanghai Aladdin Industrial Inc. Oleic acid (OA, AR), anhydrous methanol (AR), *N*,*N*-dimethylformamide (DMF, AR), and absolute ethanol (AR) were purchased from Sinopharm Chemical Reagent Co., Ltd.

2.2. Synthesis of metal–organic framework-derived zirconia-supported Keggin heteropoly composites (HSiW@ZrO_2)

In a typical synthesis, 0.51 g of $ZrCl_4$ and 0.57 g of HSiW were completely dissolved in 18 mL of DMF under stirring at room temperature for 1 h, and then, 0.3275 g of H_2-BDC was added under stirring. After the formation of a homogeneous solution under stirring, the homogeneous solution was put in a 50 mL Teflon-lined stainless-steel autoclave and heated at 120 °C in an isothermal oven for 6 h. After air-cooling the autoclave to room temperature, the resulting precursor was washed and centrifuged using ~60 mL of DMF and ~60 mL of distilled water, and finally dried in a vacuum oven at 80 °C. The resulting material is referred to as HSiW@UiO-66. At last, the obtained precursor powders were further calcined at 300 °C, 400 °C, and 500 °C for 2 h in air to prepare the nanoporous HSiW@ZrO_2-*T* catalyst, which was denoted as HSiW@ZrO_2-300, HSiW@ZrO_2-400, and HSiW@ZrO_2-500, respectively.

2.3. Instrumentation

Fourier-transform infra-red (FTIR) spectra of the as-synthesized hybrids were obtained from powdered samples on KBr pellets using a PerkinElmer Spectrum 100 over a wavenumber scanning region of 4000–400 cm^{-1} to identify the chemical groups (bonds) present in the nanocomposite. The wide-angle XRD spectra of the as-prepared composites were recorded with a D8 ADVANCE (Germany) using CuKα (1.5406 Å) radiation. The BET surface area and pore size were determined based on nitrogen adsorption–desorption isotherms using a quantachrome instrument (Quantachrome Instruments, Boynton Beach, USA). The morphology and appearance of sample catalysts were studied using a scanning electron microscope (SEM) at 2.0 kV (Hitachi S4800) and transmission electron microscope (TEM) at 200 kV (FEI Tecnai G2 20). The acidic properties of the as-synthesized HSiW@ZrO_2 hybrids were examined *via* the temperature programmed desorption of NH_3 (NH_3-TPD) using a Micromeritics, AutoChem II 2920 instrument.

2.4. Esterification experiments

The catalytic efficiency of the as-synthesized HSiW@ZrO_2 hybrids was evaluated by the esterification of OA with methanol. Initially, the OA and methanol were performed in a 50 mL stainless-steel high-pressure autoclave reactor, and proper amounts of catalyst were thoroughly dispersed in the mixture system. Then, the reaction was allowed to take place in an oil bath for an appropriate time at an appropriate temperature. Upon the completion of the reaction, the catalyst is separated from the liquid product *via* centrifugation at 8000 rpm for 5–7 min, and the liquid product is then vaporized to remove water and residual methanol. Finally, a small amount of the liquid product was measured to determine the acid value, and the acid value was determined according to the method described in ISO 660-2009 standard. The conversion of OA was estimated by measuring the acid values of the initial reactants and final products.

3. Results and discussion

3.1. Catalyst characterization

The wide-angle XRD analysis for HSiW@ZrO_2-300, HSiW@ZrO_2-400, and HSiW@ZrO_2-500 is shown in Fig. 1. XRD patterns (Fig. S1†) of HSiW@UiO-66 samples display well-defined diffraction peak characteristics of the UiO-66 frameworks, and the diffraction peaks of HSiW cannot be observed from the HSiW@UiO-66 sample, suggesting that HSiW uniform has occupied the UiO-66 cavities.[26] In the XRD analysis of HSiW@ZrO_2-300 and HSiW@ZrO_2-400, a weak broad peak is observed in the 2θ range of 15–35°, which indicates the coexistence of amorphous ZrO_2 (a-ZrO_2) and tetragonal ZrO_2 (t-ZrO_2), similar to that literature reported.[27] Notably, a strong peak at around 7.2° was observed, but the other UiO-66 peaks almost disappear, which could be related to the partial decomposition of UiO-66 to a-ZrO_2 and t-ZrO_2. In the structure of HSiW@ZrO_2-500, multiple peaks have been observed at 30.3°, 34.8°, 50.6°, and 60.0° and can be accurately assigned to the tetragonal phase of ZrO_2 (JCPDS card no. 88-1007).[28] It should be noted that the calcination temperature increase would cause

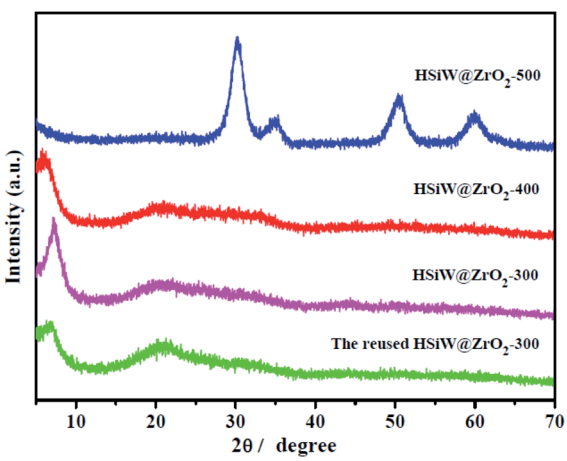

Fig. 1 Wide-angle XRD patterns of HSiW@ZrO_2-300, HSiW@ZrO_2-400, HSiW@ZrO_2-500, and the reused HSiW@ZrO_2-300 hybrids.

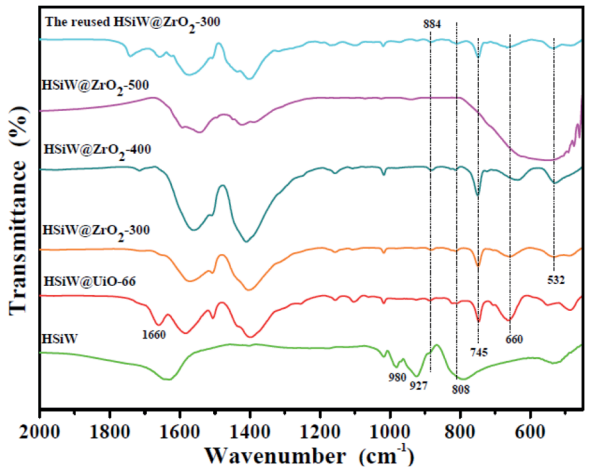

Fig. 2 FTIR spectra of the HSiW, HSiW@UiO-66, HSiW@ZrO_2-300, HSiW@ZrO_2-400, HSiW@ZrO_2-500, and the reused HSiW@ZrO_2-300 hybrids.

a deeper breaking of the UiO-66 structure, as confirmed by the disappearance of the diffraction peak at around 7.2°.

Fig. 2 shows the FTIR spectra of HSiW, HSiW@UiO-66, and the HSiW@UiO-66 at different calcination temperatures. For HSiW@UiO-66, the absorption peak at 1660 cm^{-1} is attributed to the C═O stretching vibrations of BDC carboxylic acid; however, the peak disappeared in different calcination temperature samples due to the decomposition of the organic ligand and the formation of zirconium oxide. The broad bands in the range of the 450–800 cm^{-1} region are assigned to the stretching vibrations of Zr–O or Zr–O–Zr.[29,30] In comparison with HSiW, HSiW@ZrO_2-300 and HSiW@ZrO_2-400 hybrids display specific peaks at 884 cm^{-1} (W–O_c–W) and 808 cm^{-1} (W–O_e–W) that have confirmed the existence of HSiW with the Keggin structures.[31,32] While the bands at 884 cm^{-1} and 808 cm^{-1} are not observed in the FT-IR spectra of HSiW@ZrO_2-500, it is implied that the Keggin structure is destroyed in the calcination process of 500 °C. All the results confirm the attachment of HSiW on the hybrids when the calcination

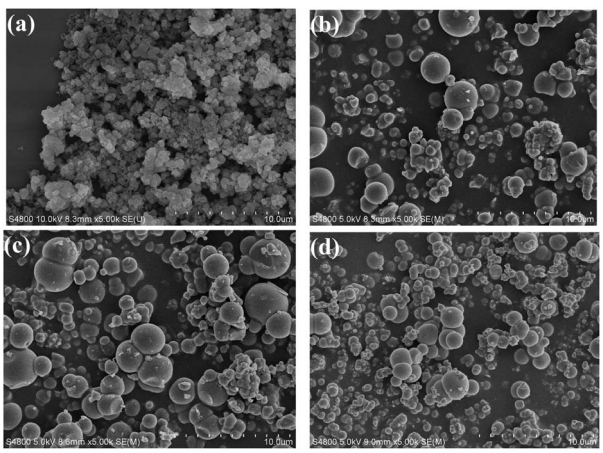

Fig. 3 SEM images for (a) HSiW@UiO-66, (b) HSiW@ZrO_2-300, (c) HSiW@ZrO_2-400, (d) HSiW@ZrO_2-500.

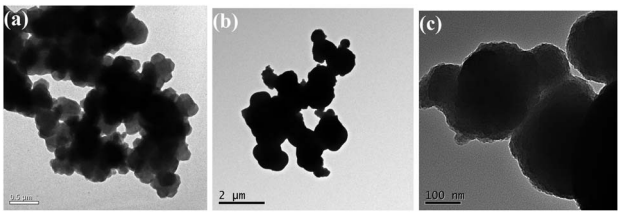

Fig. 4 Typical TEM images of HSiW@UiO-66 (a) and HSiW@ZrO_2-300 (b, c) hybrids.

temperature is at 300 °C and 400 °C. The above-mentioned results suggest the successful synthesis of HSiW@ZrO_2 hybrids.

Fig. 3a–d illustrate the SEM images of the precursor (HSiW@UiO-66) and the HSiW@UiO-66 at different calcination temperatures. From Fig. 3a, the HSiW@UiO-66 sample presents an octahedral morphology with an average crystal size of about 50–200 nm. After calcination, the obtained HSiW@ZrO_2-*T* catalysts exhibit unevenly distributed particles of spherical shapes, and the overall particle size appears to be increased from the original 0.2 μm to about 1.0 μm. This may be related to the decrease in the porous structure and organic ligands, and the atom of oxygen from the organic ligand combined with zirconium atoms and turned into zirconium oxide in the calcination process.[33,34] From Fig. 3b–d, typical SEM images also clearly show that the dispersion of HSiW@ZrO_2-300 particles is better than that of other samples. It can be explained that the particles tend to aggregate in the case of high-temperature heating; then, such good dispersion of hybrids should benefit better catalytic activity.

In this study, TEM images are also obtained to study the microstructure of these hybrids (Fig. 4a–c). As apparent from Fig. 4a and b, the as-prepared samples possess the clear porous structure due to the stacking of particles. For the HSiW@ZrO_2-300 sample, it also shows a spherical morphology (Fig. 4c), and the nonuniform large particles were surrounded by some smaller particles, which originate from the partial collapse of the UiO-66 framework during the heat treatment, similar to that reported previously.[35] The obtained results from TEM matched with the FTIR spectra and SEM images.

As shown in Fig. 5, the N_2 adsorption–desorption isotherms and pore size distribution of HSiW@UiO-66 and HSiW@ZrO_2-300 hybrids have been studied. It can be found that the tested two hybrids show a typical type-I mode, demonstrating the presence of micropores in those samples, which may be assigned to the stacking of particles with each other. Interestingly, it should be noted that the shape of the hysteresis loop profile of HSiW@ZrO_2-300 hybrids has no significant changes after being calcinated at 300 °C, suggesting that the framework structure of initial UiO-66 can be retained to a certain extent. The measured BET surface area, pore volume and mean pore size of HSiW@UiO-66 were 758.3 m^2 g^{-1}, 0.438 cm^3 g^{-1}, and 2.3 nm, respectively. After calcination, the BET surface area, pore volume and average pore size of HSiW@ZrO_2-300 are changed to 338 m^2 g^{-1}, 0.212 cm^3 g^{-1}, and 2.5 nm, respectively. Based on the above-mentioned data, the BET surface area and pore volume of HSiW@ZrO_2-300 decreases; however, it is still

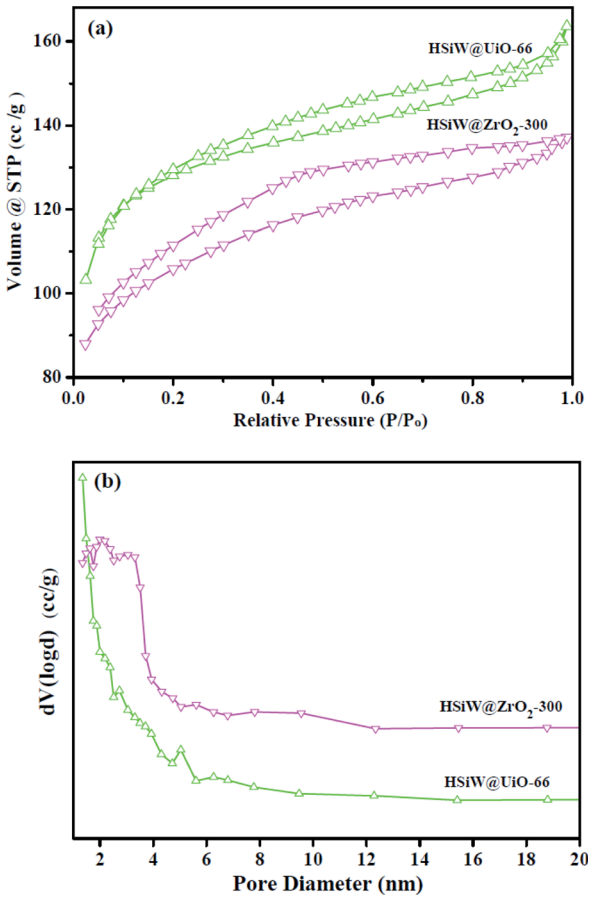

Fig. 5 (a) Profiles of the N_2 adsorption–desorption isotherm and (b) pore size distribution of HSiW@UiO-66 and HSiW@ZrO_2-300 hybrids.

a relatively high surface area, which can be explained that the presence of HSiW inhibits the excessive shrinkage of the precursor in the case of the calcination process and the formation of cavity between particles, and similar phenomenon has also been reported previously.[35,36] More significantly, relatively high surface area and good porosity would facilitate mass transfer for esterification.

In general, NH_3-TPD is widely used to characterize the acid strength and acidity of the composites. Fig. 6 shows the NH_3-TPD patterns of the HSiW@ZrO_2-300 hybrids, and the results of the NH_3-TPD analysis show that the hybrids have one weak and one strong acid desorption peak at 98 °C and 576 °C, respectively. Moreover, the total acidity capacity of the HSiW@ZrO_2-300 composite is calculated to be 6.2 mmol g^{-1}. It can be suggested that the strong acidity and high acidity capacity of the hybrids is the main factor for the esterification of OA with methanol.

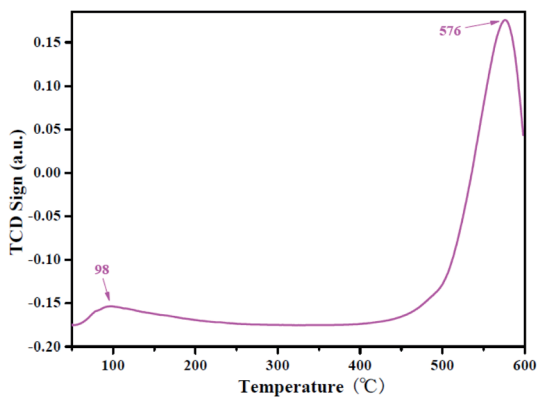

Fig. 6 NH_3-TPD patterns of HSiW@ZrO_2-300 hybrids.

3.2. Catalytic performance of different catalysts

In this study, it investigates the influence of the calcination temperature (300 °C, 400 °C, and 500 °C) on the preparation of the HSiW@ZrO_2-*T* catalyst, and the catalytic testing of OA esterification was carried out for 1–4 h under the reaction conditions: 0.15 g catalyst, 1 : 20 OA/methanol molar ratio, and a temperature of 160 °C. As depicted in Fig. 7, for all HSiW@ZrO_2 catalysts, the OA conversion can be improved by increasing the reaction time. Moreover, it is found that HSiW@ZrO_2-300 displays higher catalytic activity than HSiW@ZrO_2-400 and HSiW@ZrO_2-500. When the reaction time is 4 h, the OA conversions are 94.0%, 89.3%, and 69.8% using HSiW@ZrO_2-300, HSiW@ZrO_2-400 and HSiW@ZrO_2-500, respectively. Most probably, a moderate calcination temperature towards the generation of abundant HSiW–ZrO_2 interfaces for biodiesel production may also be due to the better particle dispersion, appropriate pore size, and relatively large specific surface area of HSiW–ZrO_2-300 as well as strong acidity. Moreover, in our previous study,[26] the catalytic activity of HSiW@UiO-66 and UiO-66 in the esterification reaction of OA with methanol was also determined, and the results showed that the OA conversions obtained are about 80.5% and 75.0% for HSiW@UiO-66 and UiO-66 samples, respectively. Therefore, the esterification parameters including the reaction temperature, catalyst amount, and OA/methanol molar ratio were evaluated over HSiW@ZrO_2-300 hybrids in the subsequent study.

3.3. Exploring the optimum reaction condition

3.3.1 Influence of the reaction temperature and time. In general, the esterification of OA and methanol using

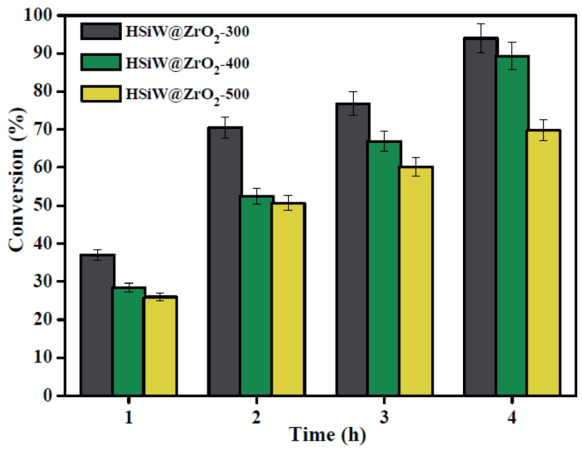

Fig. 7 Catalytic performances of the different catalysts in the esterification of OA.

a heterogeneous catalyst is a three-phase system; therefore, it is difficult for the reactant molecules to transfer from one phase to the other. However, applying a high temperature can accelerate the molecular movement, and thus decrease diffusion resistance and increase the miscibility.[37] Then, the effects of reaction temperatures at 140 °C, 150 °C and 160 °C on OA esterification are shown in Fig. 8, separately, when the OA/methanol molar ratio is 1 : 20 and the amount of catalyst is 0.15 g. Based on the results of Fig. 8, it shows that the conversion of oleic acid increases with the increase in the reaction temperature or time, and the conversion of OA increases from 62.5% to 95.4% as the reaction temperature increases from 140 °C to 160 °C for 5 h. This may be because the esterification reaction is endothermic; thus, higher temperature facilitates the esterification reaction and favors forward direction. In addition, when the reaction time ranges from 4 h to 5 h at 160 °C, in response, the conversion of OA increases from 94.0% to 95.4%, and it suggests that the excessively added reaction time has no significant effect on the conversion. Therefore, the optimum temperature and time are 160 °C and 4 h, respectively.

3.3.2 Influence of the OA/methanol molar ratio. The esterification of OA with methanol is a reversible process; thus, excess methanol can be added to form more ester. The effects of the OA/methanol molar ratio on the methyl oleate production in the range from 1 : 10 to 1 : 30 (Fig. 9a) under the reaction conditions such as 0.15 g catalyst amount, 160 °C of temperature for 4 h have been studied. As depicted in Fig. 9a, as the OA/methanol molar ratio decreased from 1 : 10 to 1 : 30, the conversion of OA increased from 63.2% to 85.9% at 2 h, indicating that the OA conversion of reversible esterification could be improved by applying excess amounts of methanol. Surprisingly, when the reaction time is 4 h, the conversion of OA increased from 94.0% to 98.2% with the OA/methanol molar ratio decreased from 1 : 20 to 1 : 30, and it indicates that the excessively added methanol has no significant effect on the OA conversion because the esterification reaction has reached a dynamic equilibrium. Moreover, the OA conversion is obtained with a molar ratio of oleic acid to methanol 1 : 120 about 92–99% for the $0.07Eu^{3+}$/BS30 catalyst, suggesting that the molar ratio of OA/methanol in our reaction is lower than or comparable to those in most reports.[38] Hence, the molar ratio of OA to methanol of 1 : 20 is the most favorable for the reaction.

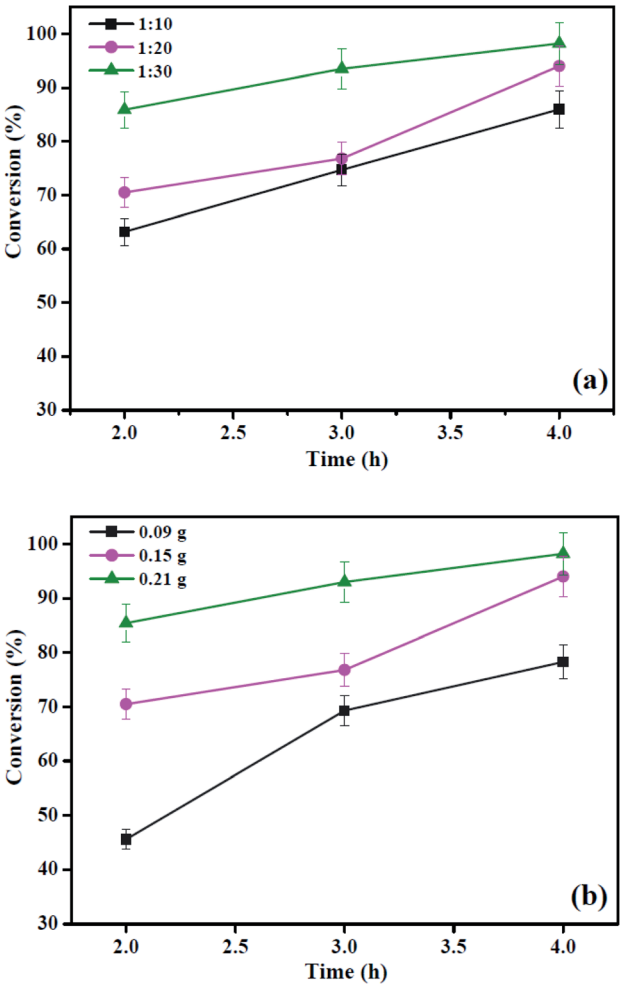

Fig. 9 Effect of (a) the molar ratio of OA to methanol (reaction conditions: a temperature of 160 °C, and catalyst amount of 0.15 g) and (b) catalyst amount (reaction conditions: a temperature of 160 °C, and the molar ratio of OA to methanol of 1 : 20).

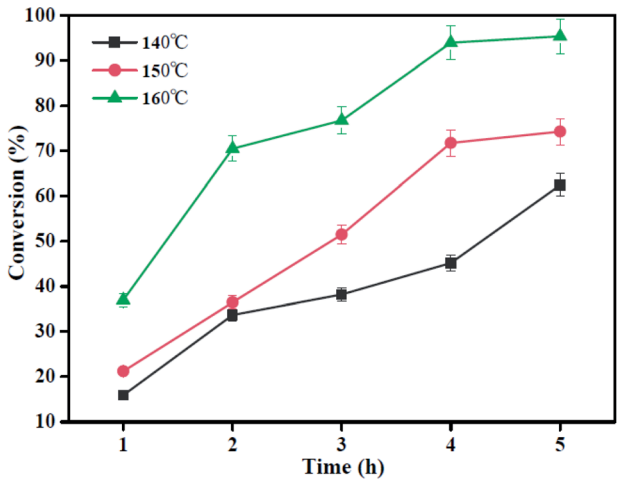

Fig. 8 Effects of the esterification time and temperature. Reaction conditions: the molar ratio of OA to methanol of 1 : 20 and catalyst amount of 0.15 g.

3.3.3 Influence of the HSiW@ZrO_2-300 loading. The varying dosage of HSiW@ZrO_2-300 hybrids from 0.09 g to 0.21 g was observed on the methyl oleate production. From Fig. 9b, with an increase in the hybrid amount, the OA conversion also increases, and this may be attributed to the availability of increasing active sites with an increase in the catalyst dosage. In addition, when the amount of catalyst is 0.15 g at 4 h, the conversion of OA is 94.0%, and at this time, no significant impact on the conversion of OA is reported after a further increase of HSiW@ZrO_2-300 hybrids, which is probable due to the limitation of the chemical reaction equilibrium. Therefore, 0.15 g is the optimum catalyst amount.

3.4. Catalytic reusability of HSiW@ZrO_2-300

The reusability test of the as-prepared HSiW@ZrO_2-300 hybrids in the esterification reaction of OA with methanol was examined at the reaction temperature of 160 °C, the molar ratio of OA/methanol of 1 : 20, and the reaction time of 4 h. After each cycle, the hybrids were separated and recovered by centrifugation, and rinsed with methanol two times. Then, the catalyst was directly used in the next cycle. As displayed in Fig. 10a, the conversion of OA after nine cycles was maintained above 82.0%. Obviously, no significant decrease in conversion can be observed, suggesting the good stability and reusability of HSiW@ZrO_2-300 hybrids used as a heterogeneous catalyst. It can also be proven that the crystallinity and chemical structure (XRD and FTIR spectra, Fig. 1 and 2) of HSiW@ZrO_2-300 remain almost stable, even after nine cycles, indicating the significant catalytic stability of HSiW@ZrO_2-300 hybrids.

Undoubtedly, the conversion was slightly decreased from the first run (94.0%) to ninth run (82.6%). To further test if the active sites impregnated into the reaction medium leads to a decrease in the catalyst activity, the hot filtration experiment was performed. The hybrids were separated from the reaction medium by filtration after 2 h (with 70.5% conversion of OA), and the filtrate was continued to react under the same reaction conditions, and the experimental results are shown in Fig. 10b. From Fig. 10b, the OA conversion remained almost consistent with the removal of the hybrids in the hot filtration experiment, which indicated that the hybrids were not the leaching active sites. Thus, a slight reduction in conversion may be due to the active sites being covered by unreacted OA and could block the active sites. Based on the results, the HSiW@ZrO_2-300 hybrids had good catalytic reusability, which is comparable to that from our previous study.[26]

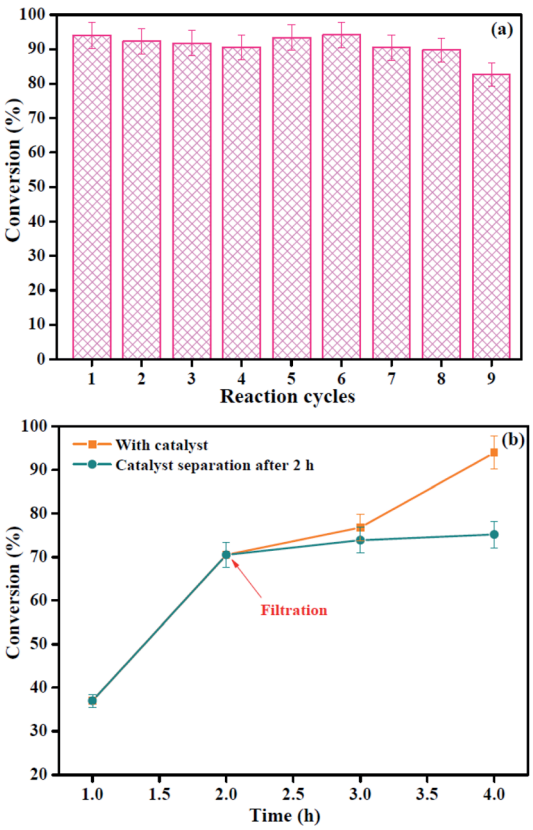

Fig. 10 (a) The OA conversion obtained by HSiW@ZrO_2-300 at nine consecutive cycles of esterification reaction; (b) hot filtration test of esterification.

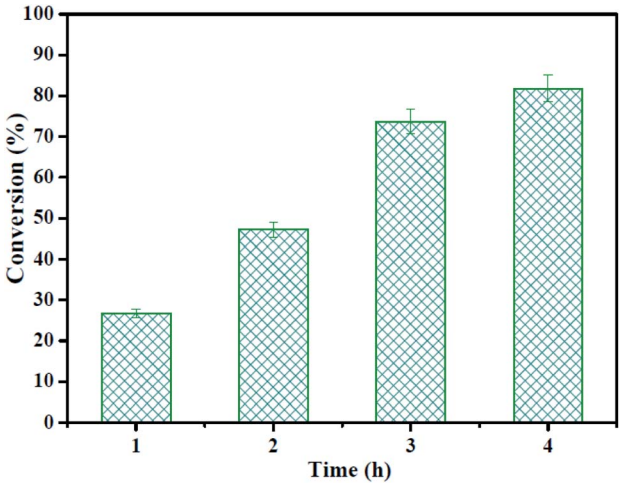

Fig. 11 Catalyst performance for the esterification of the high acid value of the *Jatropha curcas* oil. Reaction conditions: an OA–methanol molar ratio of 1 : 50, reaction temperature of 160 °C with catalyst amount of 0.15 g.

3.5. Catalytic activity of HSiW@ZrO_2-300 hybrids towards the esterification of the high acid value *Jatropha curcas* oil

Furthermore, the catalytic activity of the HSiW@ZrO_2-300 hybrids for the esterification of the high acid value of *Jatropha curcas* oil is studied, and the catalytic results are displayed in Fig. 11. The high acid value of the *Jatropha curcas* oil conversion over HSiW@ZrO_2-300 reached 81.8% after 4 h, indicating that the hybrids also exhibited excellent catalytic activities towards the pretreatment processing (esterification process) of cheap non-edible oil.

4. Conclusions

To sum up, nanoporous HSiW@ZrO_2 hybrids were successfully fabricated *via* a facile hydrothermal reaction and subsequent calcination of a HSiW-impregnated UiO-66 precursor and introduced in the esterification of OA with methanol. It was observed that the HSiW@ZrO_2 catalyst calcinated at 300 °C showed excellent catalytic activity compared to other catalysts in the conversion of OA into methyl oleate, providing a conversion of 94.0% under optimum reaction conditions. Further, the catalyst reusability study showed that the hybrids can successfully be reused in nine cycles with sufficiently high OA conversion. Interestingly, it was also found that the hybrids were effective for the esterification of the high acid value of *Jatropha curcas* oil. Overall, this study concludes that the HSiW@ZrO_2 hybrids can be used as an efficient, sustainable, prospective catalyst for the production of biofuels.

Conflicts of interest

There are no conflicts to declare.

Acknowledgements

This work was financially supported by the Guizhou Science and Technology Foundation ([2020]1Y054), the 2018 Thousand Level Innovative Talents Training Program of Guizhou Province, the Academician Workstation of Guizhou Science and Technology Plan (Guizhou S&T Cooperation Platform Talents [2016] 5602), the Science and Technology Cooperation Project of Guizhou Province (No. LH [2017]7059), the Technical Talent Support Program of Guizhou Education Department (KY [2018] 069), and the Creative Research Groups Support Program of Guizhou Education Department (KY [2017]049), and the Innovative Entrepreneurship Training Program for Undergraduates of the Guizhou Education Department (S202010667001).

Notes and references

1 C. Z. Li, X. C. Zhao, A. Q. Wang, G. W. Huber and T. Zhang, *Chem. Rev.*, 2015, **115**, 11559–11624.
2 Q. Y. Zhang, Y. T. Zhang, J. S. Cheng, H. Li and P. H. Ma, *Curr. Org. Chem.*, 2020, **24**, 1876–1891.
3 L. Zhang, K. C. Loh, A. Kuroki, Y. J. Dai and Y. W. Tong, *J. Hazard. Mater.*, 2021, **402**, 123543.
4 V. K. Booramurthy, R. Kasimani, S. Pandian and B. Ragunathan, *Environ. Sci. Pollut. Res.*, 2020, **27**, 20598–20605.
5 K. Rajkumari and L. Rokhum, *Biomass Convers. Biorefin.*, 2020, **10**, 839–848.
6 T. Roy, S. Sahani and Y. C. Sharma, *Fuel*, 2020, **274**, 117644.
7 Q. Y. Zhang, F. F. Wei, P. H. Ma, Y. T. Zhang, F. H. Wei and H. L. Chen, *Waste Biomass Valorization*, 2018, **9**, 911–918.
8 R. F. Abdullah, U. Rashid, Y. H. Taufiq-Yap, M. L. Ibrahim, C. Ngamcharussrivichai and M. Azam, *RSC Adv.*, 2020, **10**, 27183–27193.
9 Q. Y. Zhang, D. Ling, D. D. Lei, J. L. Wang, X. F. Liu, Y. T. Zhang and P. H. Ma, *Front. Chem.*, 2020, **8**, 129.
10 H. R. Mahmoud, S. A. El-Molla and M. M. Ibrahim, *Renewable Energy*, 2020, **160**, 42–51.
11 S. Tantisriyanurak, H. N. Duguid, L. Peattie and R. Dawson, *ACS Appl. Polym. Mater.*, 2020, **2**, 3908–3915.
12 C. D. Prates, F. C. Ballotin, H. Limborço, J. D. Ardisson, R. M. Lago and A. P. de Carvalho Teixeira, *Appl. Catal., A*, 2020, **600**, 117624.
13 L. Soler, A. Illanes and L. Wilson, *Catal. Today*, 2015, **259**, 177–182.
14 J. Gardy, M. Rehan, A. Hassanpour, X. J. Lai and A. S. Nizami, *J. Environ. Manage.*, 2019, **249**, 109316.
15 A. P. da Luz Corrêa, R. R. C. Bastos, G. N. da Rocha Filho, J. R. Zamian and L. R. V. da Conceição, *RSC Adv.*, 2020, **10**, 20245–20256.
16 Q. Y. Zhang, H. Li, X. F. Liu, W. T. Qin, Y. P. Zhang, W. Xue and S. Yang, *Energy Technol.*, 2013, **1**, 735–742.
17 J. Y. Chen, M. C. Li, M. T. Li, X. C. Lin and T. Qiu, *ACS Sustainable Chem. Eng.*, 2020, **8**, 6956–6963.
18 F. C. Ballotin, M. J. da Silva, R. M. Lago and A. P. de Carvalho Teixeira, *J. Environ. Chem. Eng.*, 2020, **8**, 103674.
19 M. J. da Silva, M. G. Teixeira, D. M. Chaves and L. Siqueira, *Fuel*, 2020, **281**, 118724.
20 B. Meryemoglu, *Catal. Commun.*, 2021, **149**, 106248.
21 C. B. Vilanculo, L. C. de Andrade Leles and M. J. da Silva, *Waste Biomass Valorization*, 2020, **11**, 1895–1904.
22 P. Ganji and S. Roy, *Catal. Commun.*, 2020, **134**, 105864.
23 W. L. Xie, C. L. Gao and J. B. Li, *Renewable Energy*, 2021, **168**, 927–937.
24 X. X. Xie, Y. C. Yang, B. H. Dou, Z. F. Li and G. Li, *Coord. Chem. Rev.*, 2020, **404**, 213100.
25 U. Ryu, S. Jee, P. C. Rao, J. Shin, C. Ko, M. Yoon, K. S. Park and K. M. Choi, *Coord. Chem. Rev.*, 2021, **426**, 213544.
26 Q. Y. Zhang, T. T. Yang, X. F. Liu, C. Y. Yue, L. F. Ao, T. L. Deng and Y. T. Zhang, *RSC Adv.*, 2019, **9**, 16357–16365.
27 T. K. Liu, X. L. Hong and G. L. Liu, *ACS Catal.*, 2020, **10**, 93–102.
28 N. Y. Lu, X. L. Zhang, X. L. Yan, D. H. Pan, B. B. Fan and R. F. Li, *CrystEngComm*, 2020, **22**, 44–51.
29 S. Zolfagharinia, E. Kolvari, N. Koukabi and M. M. Hosseini, *Arabian J. Chem.*, 2020, **13**, 227–241.
30 M. M. Fan, H. Liu and P. B. Zhang, *Fuel*, 2018, **215**, 541–550.
31 K. M. Parida and S. Mallick, *J. Mol. Catal. A: Chem.*, 2007, **275**, 77–83.
32 Q. Y. Zhang, D. D. Lei, Q. Z. Luo, J. L. Wang, T. L. Deng, Y. T. Zhang and P. H. Ma, *RSC Adv.*, 2020, **10**, 8766–8772.
33 Y. Chen, S. T. Li, S. Y. Lv and Y. M. Huang, *Catal. Commun.*, 2021, **149**, 106215.
34 H. Y. Wang, W. Y. Fu, Y. W. Chen, F. Y. Xue and G. Y. Shan, *Spectrochim. Acta, Part A*, 2021, **246**, 119006.
35 H. Sun, X. L. Yu, X. Y. Ma, X. Q. Yang, M. Y. Lin and M. F. Ge, *Catal. Today*, 2020, **355**, 580–586.
36 D. S. Liu, M. N. Li, X. C. Li, F. J. Ren, P. Sun and L. C. Zhou, *Chem. Eng. J.*, 2020, **387**, 124008.
37 B. Changmai, R. Rano, C. Vanlalveni and L. Rokhum, *Fuel*, 2021, **286**, 119447.
38 H. R. Mahmoud, *Fuel*, 2020, **280**, 118596.